Inorganic Chemistry

pubs.acs.org/IC

Article

Intermetallic Compound Re_2Ga_9Ge with Re- and Ge-Embedded Gallium Clusters: Synthesis, Crystal Structure, Chemical Bonding, and Physical Properties

Maxim S. Likhanov, Valeriy Yu. Verchenko, Vladislav O. Zhupanov, Zheng Wei, Evgeny V. Dikarev, Alexey N. Kuznetsov, and Andrei V. Shevelkov*

Cite This: *Inorg. Chem.* 2022, 61, 568−578

Read Online

ACCESS | Metrics & More | Article Recommendations | Supporting Information

ABSTRACT: Transition metal-based endohedral cluster intermetallic compounds are interesting electron phases, which frequently exhibit superconductivity with a peculiar interplay between the critical temperature and valence electron count. We present a new Re-based endohedral gallium cluster compound, Re_2Ga_9Ge. Its unique crystal structure ($P4_2/mmc$ space group, a = 8.0452(3) Å, c = 6.7132(2) Å) is built by two types of gallium polyhedra: monocapped Archimedean antiprisms centered by rhenium atoms and tetrahedra containing a main-group element inside. The analysis of chemical bonding shows the presence of localized pairwise interactions between the p-block elements and the formation of multicenter bonds with the participation of d-orbitals of rhenium. In the electronic band structure, the Fermi level is located in a narrow pseudogap indicating the optimum band filling and thus explaining the virtual absence of a homogeneity range. The compound exhibits Pauli paramagnetism and metallic properties with unexpectedly low thermal conductivity. A sharp anomaly observed on the magnetic susceptibility and resistivity curves presumably indicates the electronic phase transition accompanied by charge ordering at the characteristic temperature of T * = 271 K in zero magnetic field.

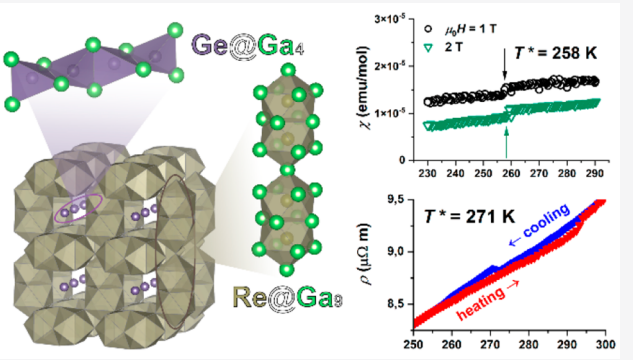

INTRODUCTION

Among a rich realm of intermetallic compounds, there is a broad group of polar intermetallics formed by a combination of a transition metal with a p-block metal or metalloid. They form an interesting family with nontrivial chemical bonding and frequently exhibit exciting functional properties. In particular, compounds enriched with a p-metal may exhibit low-temperature superconductivity with intriguing interplay between the critical temperature and valence electron count.[1] In such compounds, the p-metal forms a three-dimensional framework with large cages occupied by atoms of a transition metal. Interestingly, many of the superconducting intermetallics are based on gallium, for example, V_2Ga_5, $ReGa_5$, Rh_2Ga_9, and Mo_8Ga_{41} intermetallic superconductors.[2−5] In these compounds, atoms of a transition metal are enclosed inside endohedral gallium clusters with a large number of vertices, 8−14; such building blocks give birth to a common name of such compounds, "endohedral superconductors".

The endohedral cluster architectures demonstrate unique structural flexibility with the persistence of superconductivity in a wide range of valence electron count. Also, endohedral cluster superconductors have similar features in their electronic band structures.[3,6] Prominent d-p hybridization—the mixing of the transition metal d states with p-states of the main-group metal or metalloid—leads to the formation of strong peaks of the density of states in the vicinity of the Fermi energy. In many cases, the opening of a gap, which separates the valence and conduction bands, can be observed. When such a band gap opens at the Fermi energy, the endohedral cluster intermetallics show semiconducting properties, as in the case of $FeGa_3$ and $RuGa_3$ with a fully occupied valence band and thus saturated chemical bonds.[7,8] On the other hand, the electron-deficient phases with a high degree of electron delocalization exhibit metallic properties and, in some cases, superconductivity, as it was observed in $PdGa_5$,[9] Rh_2Ga_9, Ir_2Ga_9,[9] $ReGa_5$,[3] Mo_8Ga_{41},[10] and other Ga-rich intermetallics.

The search for new superconductors can be conducted among the endohedral cluster frameworks, and some rules that have already begun to take shape may help here. First of all, valence electron count (VEC) should be taken into account for

Received: October 18, 2021
Published: December 21, 2021

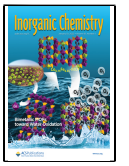

https://doi.org/10.1021/acs.inorgchem.1c03240
Inorg. Chem. 2022, 61, 568−578

the rational design of new superconducting materials. Many intermetallic frameworks are found in the vicinity of some magic values of VEC that define the islands of stability. For example, within the large families of Heusler compounds[11] and Nowotny chimney ladder phases,[12] such basic values of VEC can be found. The modern concept is based on the 18-*n* rule,[13] which explains the appearance of magic values of VEC on the basis of stable electronic configurations and analogies to molecular complexes of transition metals.[14] However, superconducting materials typically exist outside of the islands of stability. Indeed, there is a conjecture on the competition between structural stability and superconductivity, and the superconducting endohedral cluster frameworks are often the electron deficient phases with respect to the compounds with precise VEC.[1,3] The manipulation of VEC is possible when several elements from different groups of the periodic table are treated together, and their ratio can be adjusted.

When several main-group elements are combined in one endohedral cluster framework, new compounds can be synthesized, and even unknown structure types can be discovered. For example, two endohedral gallium cluster superconductors, Mo_8Ga_{41}[15] and Mo_6Ga_{31},[16] are known in the Mo−Ga binary system, while the combination of gallium and zinc expands the family of superconductors due to the formation of the $Mo_8Ga_{41-x}Zn_x$ solid solution. Furthermore, the $Mo_7Ga_{52-x}Zn_x$ ternary compound with a quasicrystal approximant endohedral cluster framework and surprisingly narrow homogeneity range was discovered in the Mo−Ga−Zn ternary system.[17] Mixing gallium and tin was used to synthesize new superconducting compounds $Mo_8Ga_{41-x}Sn_x$ and $Mo_4Ga_{21-x-\delta}Sn_x$,[18] and also, a family of the $Mo_4Ga_{20}E$ superconductors was discovered, where nontransition elements E = S, Se, Te, or Sb occupy the cuboctahedral cages of the endohedral gallium cluster framework.[19]

In a similar fashion, Re-based intermetallic compounds have been discovered by combining gallium with other elements, such as zinc and germanium. In the Re−Ga binary system, only the $ReGa_5$ endohedral cluster superconductor has been discovered.[3] On the other hand, crystal growth from the mixed flux of gallium and zinc metals yields two previously unknown ternary compounds: the $ReGa_3Zn$ narrow-gap semiconductor and metallic $Re_8Ga_{41-x}Zn_x$, which is isostructural with Mo_8Ga_{41}.[20] When using the flux of gallium with tin, lead, or bismuth, crystals of the $ReGa_{\sim 5}M$ (M = Sn, Pb, Bi) ternary compounds can be isolated.[21] In the Re−Ga−Ge system, two narrow-gap semiconductors, $ReGa_2Ge$[22] and $ReGaGe_2$,[23] with endohedral cluster frameworks formed by gallium and germanium species, were recently discovered. Also, in the Re−Ga−Si system, semiconducting ReGaSi with a close-packed structure derived from the $MoSi_2$-type was obtained.[24,25]

Synthesis of endohedral cluster intermetallic compounds can be performed from a high-temperature melt based on the excess of a low-melting metal, the so-called flux method, that enables the growth of crystals of excellent quality. A combination of several low-melting metals within the joint flux technique can be used for the exploratory synthesis of previously unknown endohedral cluster compounds with intriguing functional properties.[18,20] In this paper, we report on the synthesis of a new ternary intermetallic compound, Re_2Ga_9Ge, obtained by the flux method from the mutual excess of gallium and germanium. We present its unique crystal structure with the Re- and Ge-embedded gallium clusters, features of the electronic structure and chemical bonding, as well as magnetic and transport properties.

EXPERIMENTAL SECTION

Synthesis and Characterization. Rhenium powder (99.99%, Sigma-Aldrich), germanium chips (99.999%, Sigma-Aldrich), and gallium ingots (99.9999%, Sigma-Aldrich) were used as starting materials. The crystal growth of Re_2Ga_9Ge was carried out using the mixed flux of gallium and germanium. The mixture of elements with a molar ratio of Re:Ga:Ge = 1:(50−*x*):*x* (*x* = 2.5, 5, and 10, 1 g total mass) was placed in quartz ampules, which were evacuated, sealed, and annealed in a muffle furnace. The temperature regime included heating to 1273 K and annealing at this temperature for 48 h followed by slow cooling at the rate of 4 K h^{-1} to 673 K. An excess of gallium was removed by centrifugation at 333 K using a Hettich EBA 280 centrifuge; gallium residues were dissolved in 0.1 M hydrochloric acid for 12 h. Synthesis of Re_2Ga_9Ge as a polycrystalline sample was performed by the standard ampule technique. Starting materials taken in the stoichiometric amounts were annealed inside an evacuated silica ampule at 1223 K for 24 h, cooled to 773 K, and kept at this temperature for 5 d. After this temperature regime, the polycrystalline sample was thoroughly ground in an agate mortar, pressed into a pellet, and annealed again at 773 K for 14 d.

All samples were examined by powder X-ray diffraction (PXRD) using a Huber G670 Guinier Camera (Cu Kα1 radiation, Ge monochromator, λ = 1.5406 Å). The data were collected by scanning the image plate 4 times after an exposure time of 2400 s at room temperature. Elemental composition of the obtained crystals was determined on a scanning electron microscope JSM JEOL 6490-LV equipped with an energy dispersive X-ray (EDX) analysis system INCA x-Sight. The decomposition temperature of Re_2Ga_9Ge was determined employing differential scanning calorimetry on a STA 409 PC Luxx thermal analyzer (Netzsch). The polycrystalline sample was heated from room temperature to 1073 K at the rate of 10 K min^{-1} in argon gas flow (high purity Ar, 99.998%).

Crystal Structure Determination. Single crystals of Re_2Ga_9Ge were investigated on a Bruker D8 VENTURE single-crystal X-ray diffractometer equipped with a PHOTON 100 CMOS detector, graphite monochromator, and Mo X-ray tube (λ = 0.73071 Å). The frame width of 0.50° and exposure time of 15 s/frame were employed for data collection. Data reduction and integration were performed with the Bruker software package SAINT (Version 8.38A).[26] The absorption was corrected using the multiscan routine as implemented in SADABS (Version 2016/2).[27,28] The crystal structure was solved by the charge-flipping algorithm using the Superflip program.[29] Further, the data were refined in the full-matrix anisotropic approximation against $|F^2|$ using the SHELXL program (version 2018/3).[30] The crystal structure was visualized using the VESTA program.[31] Crystallographic data as well as structure solution and refinement details are presented in Tables 1 and 2.

For the single-phase polycrystalline sample of Re_2Ga_9Ge, the crystal structure was refined using the Rietveld method in the Jana2006 program.[32] PXRD was measured using a Panalytical X'pert^3 Powder diffractometer (Cu Kα1, 2, 1.54051, 1.54433 Å; PIXcel1D Medipix detector). Crystallographic data obtained for the Re_2Ga_9Ge polycrystalline sample are shown in the Supporting Information (Table S1 and Table S2). According to the refinement results, the crystal structure of the powdered sample coincides with the single-crystal structure. Figure 1 shows the PXRD pattern of Re_2Ga_9Ge and difference curve obtained during refinement.

Electronic Structure Calculations and Bonding Analysis. Electronic structure calculations were performed on the Density Functional Theory (DFT) level using the all-electron full-potential linearized augmented plane wave method (FP-LAPW) as implemented in the ELK code version 7.1.14.[33] The PBESol exchange-correlation functional[34] of the GGA-type was utilized. The Brillouin zone sampling was performed using the 8 × 7 × 7 *k*-point grid (175 irreducible *k*-points), the muffin-tin sphere radii for the respective atoms were (Bohr) 2.46 (Re), 2.29 (Ga), and 2.29 (Ge), and the

https://doi.org/10.1021/acs.inorgchem.1c03240
Inorg. Chem. 2022, 61, 568−578

Table 1. Crystallographic Data and Refinement Parameters for Re_2Ga_9Ge

formula	Re_2Ga_9Ge
formula weight ($g \cdot mol^{-1}$)	1072.50
crystal system	tetragonal
space group	$P4_2/mmc$
a (Å)	8.0452(3)
c (Å)	6.7132(2)
V (Å^3)	434.51(3)
Z	2
ρ_{calc} ($g \cdot cm^{-3}$)	8.197
μ, mm^{-1}	58.447
temperature (K)	100(2)
radiation, λ (Å)	Mo Kα, 0.71073
absorption correction	multiscan
θ range (deg)	3.581−37.810
index ranges	$-13 \le h \le 13$
	$-13 \le k \le 13$
	$-11 \le l \le 11$
N collected	28216
N unique/N observed [$I > 3\sigma(I)$]	687/648
R_1 [$I > 3\sigma(I)$]	0.0210
wR_2 [all data]	0.0398
GoF	1.28
residual electron density ($\bar{e}$ Å^{-3})	2.029/−2.039

maximum moduli for the reciprocal vectors k_{max} were chosen so that $R_{MT}k_{max} = 10.0$. The convergence of the total energy with respect to the k-point sets was checked.

Atomic coordinates and unit cell parameters obtained from the single-crystal X-ray diffraction experiment were used for electronic structure calculations. Band structure calculations were performed using two models: (i) the ordered model and (ii) the model with statistical distribution of gallium and germanium over the p-element sites, with the occupancy ratio of 9:1 for each position. In the latter case, the electronic structure was calculated within the virtual crystal approximation (VCA), where the fractional atoms with a nuclear charge of 31.1 were used for all p-element sites.

Atomic charges were calculated according to Bader's QTAIM approach.[35] The electron localizability indicator (ELI-D) was calculated according to the literature[36−38] using the DGrid 4.6 package.[39] For these two types of calculations, the ELK program version 3.1.12 was used to obtain wave functions, with all other computational conditions being the same as for the electronic structure calculations.

Transport and Thermodynamic Properties. Physical properties were measured on pellets pressed from a polycrystalline sample at the external pressure of 1.5 kbar at room temperature. Magnetization and heat capacity measurements were performed on a cylindrical pellet with the diameter and height of 3 mm and 1 mm, respectively. Magnetization was measured using the Vibrating Sample Magnetometry setup of the Physical Property Measurement System (PPMS, Quantum Design) in the temperature range of 10−380 K in 1 and 2 T magnetic fields. Heat capacity measurements were conducted on a relaxation-type calorimeter using the Heat Capacity option of PPMS. The long-pulse technique was employed,[40] in which heat pulses of a 30% temperature rise and 3τ measurement time were used, where τ is the first-order relaxation time constant. Measurements were performed by raising the temperature from 1.8 to 30 K in zero magnetic field. The dual-slope analysis of the heat capacity data was performed in the PPMS MultiVu program (Quantum Design). The low-temperature heat capacity was fitted by the equation $c_p(T) = \gamma T + \beta T^3 + \delta T^5$, yielding $\gamma = 5.25(5)$ mJ mol^{-1} K^{-2}, $\beta = 0.191(3)$ mJ mol^{-1} K^{-4}, and $\delta = 2.81(3)$ μJ mol^{-1} K^{-6}. Transport properties, including electrical resistivity, thermal conductivity, and Seebeck coefficient, were measured on the rectangular-shaped pellet with the dimensions of 8 × 3 × 2 mm^3 using the Thermal Transport option of PPMS at temperatures between 10 and 400 K in zero magnetic field.

RESULTS AND DISCUSSION

Synthesis and Crystal Structure. Exploratory syntheses performed in the Re−Ga−Ge system using joint flux of gallium and germanium yielded well-formed single crystals of ternary intermetallic compounds, which composition varied with the initial Ga/Ge ratio. During the post-treatment of reaction products, the excess of gallium could be easily removed, while the unreacted germanium was present in a mixture with crystals of ternary compounds. These crystals were carefully selected for further PXRD and EDX studies; PXRD patterns of the reaction products for different initial Ga/Ge ratios are given in Figure S1 of the Supporting Information. The sample with a starting molar ratio of elements Re:47.5Ga:2.5Ge contained the $ReGa_{5-y}Ge_y$ solid solution as a main reaction product, where $ReGa_5$ was the previously known endohedral gallium cluster superconductor.[3] According to the EDX analysis, the germanium content varied in these crystals from <1 to 3.5 at. %, which corresponds to $ReGa_{5-y}Ge_y$ with $y \le 0.21(2)$. When the initial germanium content was increased (Re:45Ga:5Ge and Re:40Ga:10Ge ratio of elements), the reaction products contained both the $ReGa_{5-y}Ge_y$ solid solution and crystals of a title compound, which crystallizes in a previously unknown structure type as will be shown below. Several crystals were tested using EDX. They all possessed the same $Re_{1.98(2)}Ga_{9.02(2)}Ge_{1.00(4)}$ elemental composition, which was also confirmed by EDX for a single crystal selected for structural studies.

Synthesis of polycrystalline Re_2Ga_9Ge was carried out using the standard ampule technique. It should be noted that the formation of the target compound was observed only at low annealing temperatures. According to the DSC analysis, Re_2Ga_9Ge melts incongruently at 650(10) °C (see Figure S2 of the Supporting Information).

Re_2Ga_9Ge showed no noticeable homogeneity range, because the increase of germanium content led to the formation of secondary phases. According to PXRD, the Re_2Ga_9Ge polycrystalline sample was single-phase, while the sample with the initial ratio of elements 2Re:8Ga:2Ge contained the target compound together with elemental

Table 2. Atomic Coordinates and Thermal Displacement Parameters for the Crystal Structure of Re_2Ga_9Ge

atom	Wyckoff site	x	y	z	U_{eq}, Å^2
Re1	4m	0.31059(3)	0	0	0.00379(5)
Ge1	2e	0.5	0.5	0.25	0.00675(16)
Ga1	8n	0.21195(5)	0.21195(5)	0.25	0.00671(9)
Ga2	4l	0.26491(9)	0.5	0.5	0.00644(12)
Ga3	4i	0	0.5	0.17988(11)	0.00676(12)
Ga4	2b	0	0	0	0.00634(17)

https://doi.org/10.1021/acs.inorgchem.1c03240
Inorg. Chem. 2022, 61, 568−578

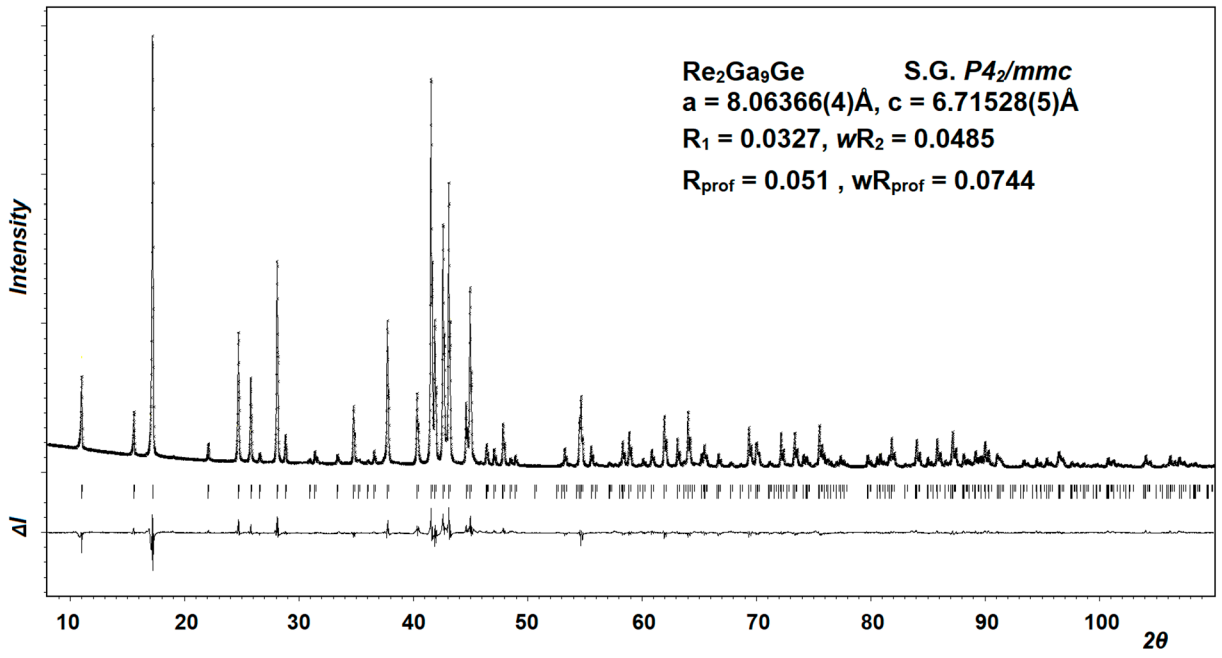

Figure 1. Powder X-ray diffraction pattern of Re_2Ga_9Ge. The upper black line represents the experimental diffraction pattern, the black ticks show peak positions, and the lower black line is the difference between the experimental and calculated patterns.

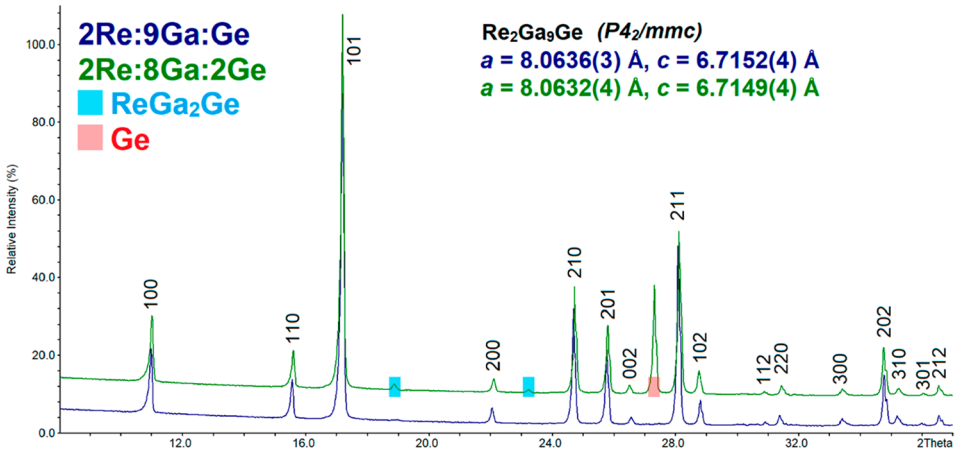

Figure 2. PXRD patterns of the polycrystalline samples with a nominal molar ratio of elements 2Re:9Ga:Ge and 2Re:8Ga:2Ge.

germanium and $ReGa_2Ge$[22] (Figure 2). The unit cell parameters of the target phase did not alter with the initial composition of the sample.

The absence of the homogeneity range of Re_2Ga_9Ge, despite similar atomic sizes of gallium and germanium and their neighboring positions in the Periodic Table, is not surprising. Similar behavior was observed earlier, when we discovered three compounds in the Re−Ga−Ge system: $ReGa_2Ge$,[22] $ReGaGe_2$,[23] and $ReGa_{0.4}Ge_{0.6}$,[41] which also showed no noticeable homogeneity range.

The crystal structure of Re_2Ga_9Ge, which is shown in Figure 3, was studied using single-crystal X-ray diffraction. Re_2Ga_9Ge can be classified as an endohedral gallium cluster compound. In the crystal structure, there are two types of polyhedra formed by gallium atoms: one-capped Archimedean (square) antiprisms centered by rhenium atoms and tetrahedra with germanium atoms inside. There are 6 independent atomic positions in the structure, one of which is occupied by rhenium, and 5 others which are occupied by the *p*-elements atoms (Table 2).

Although the single-crystal X-ray diffraction analysis cannot distinguish germanium and gallium, we assume that the 2*e* crystallographic site in the center of gallium tetrahedron is occupied by germanium. Several factors support this ordered model. First, the absence of a noticeable homogeneity range indicates the selective occupation of a certain position by germanium rather than statistical mixing of Ga/Ge atoms on different crystallographic sites. Second, the multiplicity of the 2*e* site located in the center of tetrahedron is in good agreement with the composition determined by EDX, when the ordered model is taken into account. Finally, the Ge−Ga distance of 2.53 Å is similar to those found in other $[GeGa_4]$ tetrahedra, for instance in LiGaGe.[42] Generally, in the crystal structures of related *p*-element-rich phases, the tetrahedral coordination is typical for germanium but not for gallium. For example, the tetrahedral environment of germanium is

https://doi.org/10.1021/acs.inorgchem.1c03240
Inorg. Chem. 2022, 61, 568−578

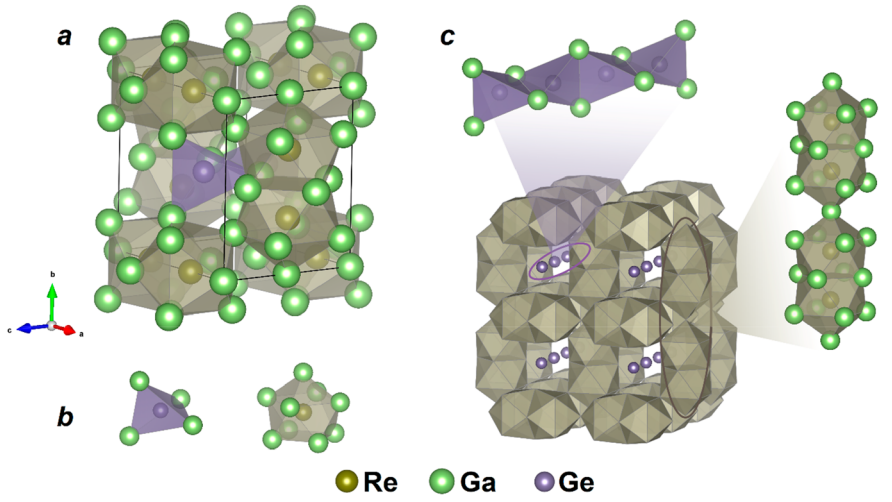

Figure 3. Crystal structure of Re_2Ga_9Ge: (*a*) the unit cell, (*b*) $Ge@Ga_4$ tetrahedron and $Re@Ga_9$ one-capped Archimedean antiprism, and (*c*) polyhedral representation highlighting $Re@Ga_9$ pairs, which share faces and vertexes and chains of $Ge@Ga_4$ tetrahedrons with common edges.

observed in $IrGe_4$[43] as well as in elemental germanium (the diamond structure type). At the same time, gallium prefers large coordination numbers both in its metallic state (*α*-Ga, space group *Cmce*)[44] and in many endohedral cluster compounds: $FeGa_3$, Mo_8Ga_{41}, etc.[7,10] It should be noted that there is no direct evidence of the segregation of germanium in the 2*e* crystallographic position. Nevertheless, we will suppose the ordered model in future considerations of crystal and electronic structures, chemical bonding, and physical properties.

Let us consider in detail the crystal structure of Re_2Ga_9Ge. The selected interatomic distances in Re_2Ga_9Ge are presented in Table 3. $Re@Ga_9$ polyhedra are stitched together along the common rectangular face forming a double cluster architecture Re_2Ga_{14}. The Re−Ga distances within the polyhedron are in the typical range of bond lengths in related $ReGa_5$ and $ReGa_{\sim 5}$(M) compounds.[3,21] The distance between the adjacent rhenium atoms exceeds 3 Å. The Re_2Ga_{14} fragments are connected to each other by the caps (Ga4), such that columns are formed (Figure 3c), which span along the *a* and *b* axes of the tetragonal unit cell. These columns alternate with each other and share common vertices (Ga1 atoms). In addition, the columns are interconnected by a relatively short Ga3−Ga3 bond of 2.41 Å, which perfectly matches the short distance between atoms in elemental gallium.[44] Within the arrangement of the columns, spacious channels are formed along the *c* axis, in which the germanium atoms are located. These atoms additionally connect the $\{Re_2Ga_{13}\}$ columns forming chains of $\{Ge@Ga_{4/2}\}$ tetrahedra. At the same time, the chains of tetrahedra are completely isolated from each other and penetrate the entire framework along the *c* axis. The $Ge@Ga_4$ tetrahedra have common edges and rotate by the angle of 90° relative to each other throughout the chain. This situation is similar to SiS_2, where the chains and fragments, containing distorted edge-sharing $Si@S_4$ tetrahedra, can be found in the crystal structures of ambient- and high-pressure polymorphs.[45]

Table 3. Selected Interatomic Distances (Less than 3.1 Å) for Re_2Ga_9Ge

atom	atom	distance, Å
Re1	Re1 (×1)	3.0476(5)
	Ga1 (×4)	2.5208(2)
	Ga2 (×2)	2.6200(6)
	Ga3 (×2)	2.6348(6)
	Ga4 (×1)	2.4988(3)
Ge1	Ga2 (×4)	2.5286(6)
Ga1	Ga2 (×2)	2.8928(4)
	Ga3 (×2)	2.9155(2)
	Ga4 (×2)	2.9381(4)
Ga3	Ga3 (×1)	2.4142(15)
	Ga2 (×2)	3.0270(8)

A polyhedron in the form of a capped Archimedean antiprism (or its slightly distorted shape) is frequently observed in endohedral gallium cluster frameworks. It is the main structural unit in $ReGa_5$[3] and its substituted analogs, $ReGa_{\sim 5}$(Bi/Sn/Pb).[21] It is also found in the crystal structures of Rh_2Ga_9[4] and Mn_6Ga_{29}[46] intermetallic compounds. Figure 4 shows a comparison of the crystal structures of endohedral gallium cluster compounds containing $T@Ga_9$ polyhedra as structural units. Notably, the crystal structures of Re_2Ga_9Ge and $ReGa_5$ have similar features: they contain the same Re_2Ga_{14} fragments connected by vertices. In $ReGa_5$, all Re_2Ga_{14} units are codirectional along the *b* axis of the orthorhombic unit cell. The introduction of germanium results in another type of polyhedron, the $Ge@Ga_4$ tetrahedron, within the Re_2Ga_9Ge endohedral cluster framework.

The combination of two polyhedra, one of which is centered by a transition metal and the other one by a *p*-element, is much less common. Only a few examples are known among the endohedral gallium cluster compounds, for instance, Mo_8Ga_{41}, where $Mo@Ga_{10}$ polyhedra together with $Ga@Ga_{12}$ cuboctahedra build the framework.[5] Furthermore, the simultaneous presence of capped Archimedean antiprisms and tetrahedra in the crystal structure of Re_2Ga_9Ge is unique for such systems. Apparently, germanium plays an important role in the formation of the discovered structural motif, which, in spite of its proximity to gallium, is more prone to the formation of covalent bonds in an intermetallic compound. The presence of germanium inside the tetrahedral cages yields strong cross-linking of the Re_2Ga_{14} columns, which also strengthens our assumption in favor of the ordered model.

https://doi.org/10.1021/acs.inorgchem.1c03240
Inorg. Chem. 2022, 61, 568−578

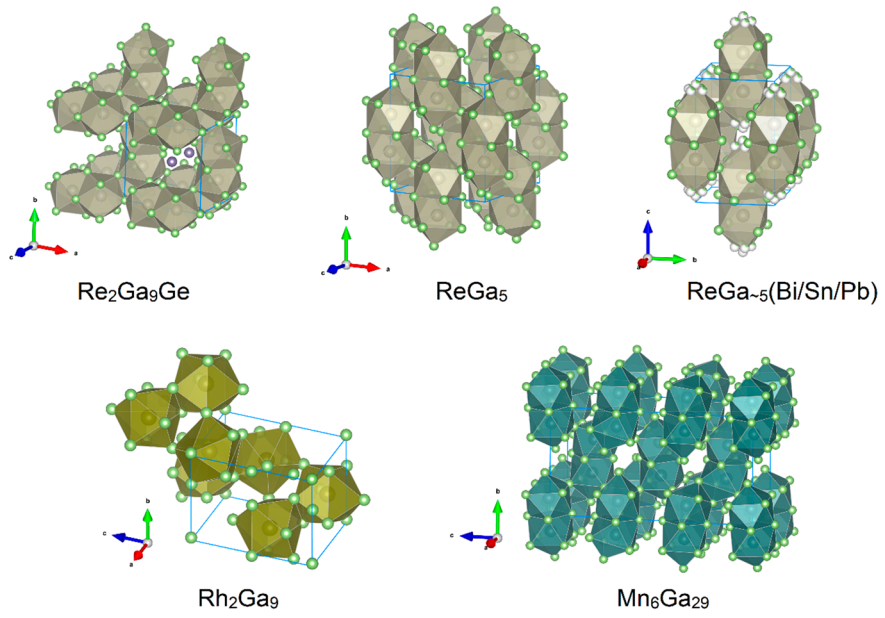

Figure 4. Comparison of the T@Ga_9 polyhedra in endohedral gallium cluster compounds: Re_2Ga_9Ge, $ReGa_5$, $ReGa_{\sim 5}$(Bi/Sn/Pb), Rh_2Ga_9, and Mn_6Ga_{29}.

Electronic Structure and Chemical Bonding. To establish the specific features of chemical bonding, we performed electronic structure calculations for Re_2Ga_9Ge. The crystal structure details presented in Tables 1 and 2 were used for electronic structure calculations. The calculated total and projected densities of states (DOS) near the Fermi energy are shown in Figure 5 both for the ordered model and assuming the statistical distribution of gallium and germanium across all *p*-element sites. The partial DOS curves are shown in Figure S3 of the Supporting Information. At the relative energies between −8 and 5 eV, the density of states is predominantly formed by the Re 5d and Ga/Ge 4p contributions.

As seen from Figure 5, the projected Re and p-metal DOS show a significant degree of mixing of the *d*- and *p*-states near the Fermi level, which might indicate prominent covalency (see also Figure S3). The DOS plots calculated for both ordered and VCA models are very similar and predict metallic behavior of Re_2Ga_9Ge due to the nonzero DOS at the Fermi level. However, regardless of the used model, we found an important feature, i.e., the Fermi level is located in a pseudogap of the DOS. The appearance of a pseudogap at the Fermi energy was previously observed in a number of endohedral gallium cluster superconductors.[3] This special feature of the electronic structure is often considered as an indication of a particular structural stability of an intermetallic framework.[3,13,14] Based on the same arguments, we assume that the location of the Fermi level in the vicinity of the pseudogap may indicate a special stability of the Re_2Ga_9Ge structure with respect to its elemental composition and valence electron count, which is supported by the fact that this compound has no noticeable homogeneity range. The fact that for fixed Re_2Ga_9Ge composition the Fermi level is in the pseudogap means that the compound has an optimal valence electron count,[13,14] i.e., the number of valence electrons in Re_2Ga_9Ge enables filling of the bands below the pseudogap, while all the states above it remain unoccupied. Electronic structure calculations that include spin−orbit coupling yielded the same band structure plots (see Figure S4), which also show the presence of a pseudogap at the Fermi energy. Calculated Bader

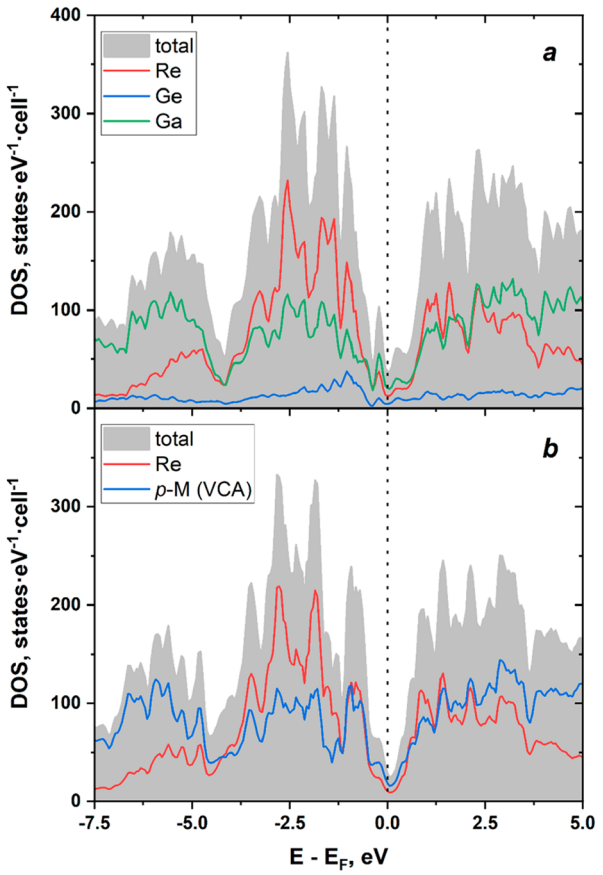

Figure 5. Total and projected density of states (PDOS) near the Fermi level for Re_2Ga_9Ge: red − Re PDOS, green − Ga PDOS, blue − Ge PDOS. (a) Ordered model and (b) mixing of gallium and germanium treated within the VCA approach. The position of the Fermi level is indicated by the dotted vertical line.

https://doi.org/10.1021/acs.inorgchem.1c03240
Inorg. Chem. 2022, 61, 568−578

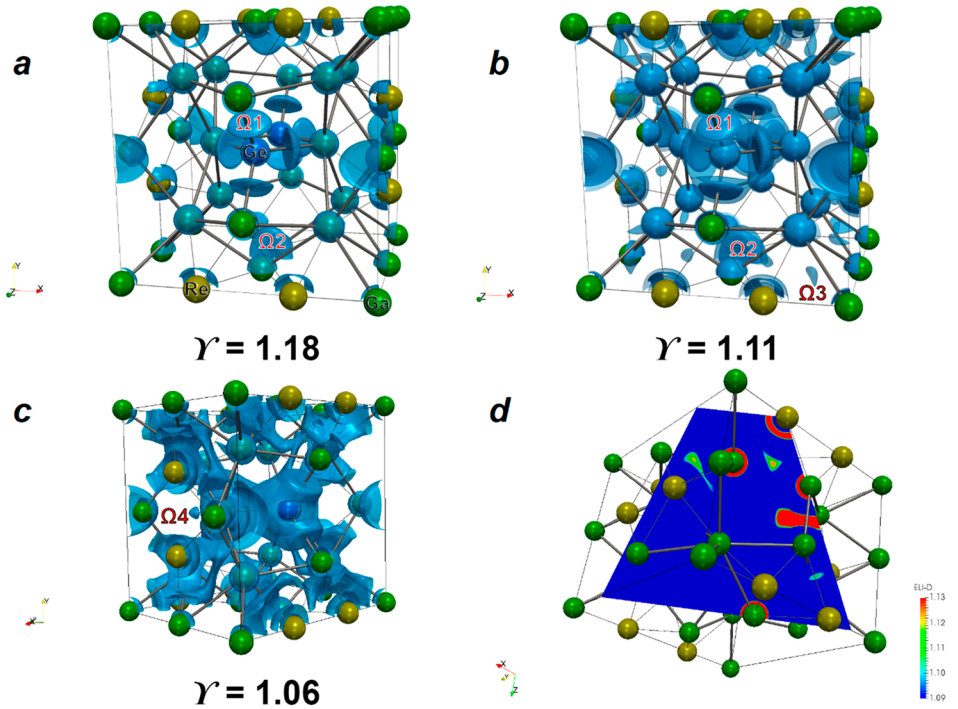

Figure 6. Calculated ELI-D topology for the ordered model of Re_2Ga_9Ge in the descending order of localizability indicator: ϒ = 1.18 (*a*), 1.11 (*b*), and 1.06 (*c*); three-centered interaction Re−Ga−Ga, highlighted in the cross section, the color shows the value of localizability indicator of ELI-D (*d*). For the explanation of Ω1−Ω4, see the text.

charges for the ordered model are ca. +0.2 (Ga), ca. −0.3 (Ge), and ca. −0.7 (Re), which also indicate significant covalency in the structure and the lack of strong ionicity.

The analysis of the ELI-D topology for the ordered model shows the presence of pairwise interactions between the *p*-block elements as well as the formation of multicenter interactions with the participation of rhenium and *p*-elements (Figure 6).

While scanning down the ϒ values, the first nonatomic attractors to appear (at ϒ = 1.18) correspond to pairwise Ge−Ga (Ω1) interactions with a population of 1.93 electrons, with respective localization domains having a slightly asymmetric disk-like shape. This asymmetry indicates a small polarity of the bond and a shift of electrons toward germanium atoms. Ga−Ga (Ω2) pair interactions are characterized by symmetric disk-shaped basins with a population of 1.47 electrons (Figure 6a). Ω2 corresponds to the shortest Ga3−Ga3 bond of 2.41 Å (see Table 3). Two-center interactions between rhenium and gallium or germanium, in contrast to $ReGaGe_2$,[23] are not observed; however, multicentered bonds are formed with the participation of rhenium *d*-electrons. Three-center interaction Re−Ga−Ga reveals Ω3 (population ∼1.07−1.2 electrons), which has an asymmetric shape, and the domain is not located in the perfect center of the triangle, which indicates slightly unequal contributions of atoms (Figure 6b and c). Another multicenter interaction observed at ϒ = 1.06 is the three-center bond 2Re + Ga (Ω4) with a population of ∼0.49 electron, located strictly in the center of the triangle (see Figure 6c). Apparently, such a localization of covalent chemical bonds may be the reason for the formation of a pseudogap in the Re_2Ga_9Ge band structure. However, the participation of rhenium in delocalized multicenter interactions, which facilitate higher electron mobility, prevents the opening of the real band gap, and as a consequence, metallic properties are predicted for the compound and further confirmed by the transport measurements (*vide infra*). This is in contrast with the behavior of another compound in the Re−Ga−Ge system, $ReGa_2Ge$, which features the localized bonding, opening of the real band gap, and thus, semiconducting properties.[22]

Physical Properties. According to the measured thermodynamic and transport properties, Re_2Ga_9Ge is a Pauli paramagnetic metallic conductor with several special features. After applying the core diamagnetism correction,[47] the magnetic susceptibility of Re_2Ga_9Ge, which is presented in Figure 7, is positive and shows very weak temperature dependence above 100 K. At low temperatures, the small upturn of magnetic susceptibility is probably caused by minor paramagnetic impurities present in the sample. In the intrinsic region, the step-like anomaly was observed at the temperature of T^* = 258 K, which is reproducible in different applied magnetic fields. A careful examination of the electrical resistivity in the same temperature range confirmed the step-like anomaly at T^* = 271 K registered on cooling and revealed the noticeable hysteresis of resistivity between 258 and 294 K in zero magnetic field. It should be noted that we detected no structural transformation between 100 and 300 K according to the refinements of crystal structure. Single-crystal data were collected at 100 K below the transition (Table 1). Further, the obtained structural model, which is presented in Tables 1 and 2, was used for the Rietveld refinement against the room-temperature PXRD data above the temperature of transition, and we found good agreement between the two data sets (Figure 1). Presumably, the observed anomaly is due to the charge ordering of Ga and Ge atoms, for which the crystallographic site ordering can also be proposed based on the observed coordination numbers, interatomic distances, and features of the electronic structure. Charge ordering is usually observed in the metallic strongly correlated systems, including

https://doi.org/10.1021/acs.inorgchem.1c03240
Inorg. Chem. 2022, 61, 568−578

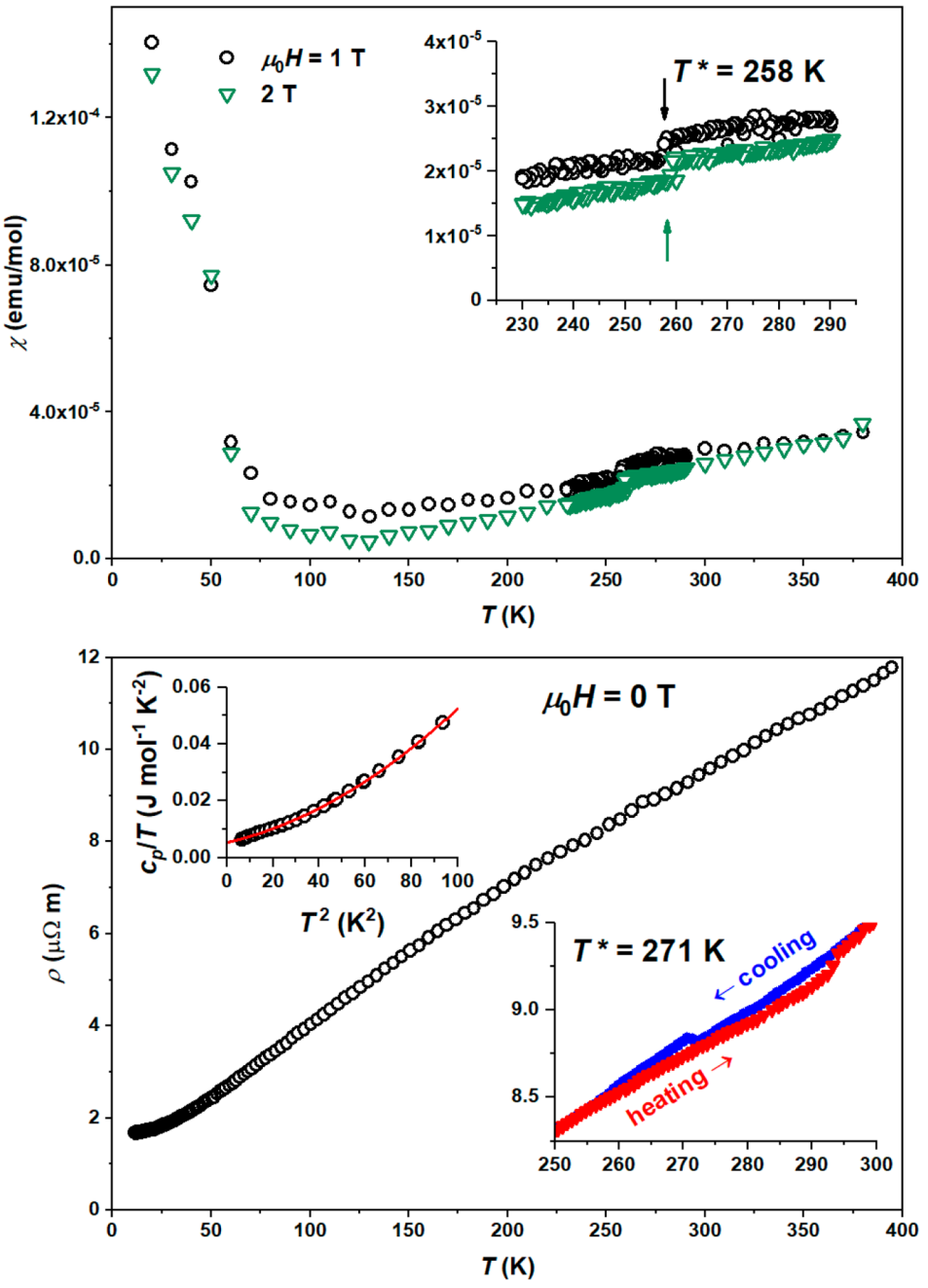

Figure 7. (top) Magnetic susceptibility of Re_2Ga_9Ge in 1 T (circles) and 2 T (triangles) magnetic fields. The inset shows the region in the vicinity of the step-like anomaly. (bottom) Electrical resistivity of Re_2Ga_9Ge measured in zero magnetic field. The lower right inset shows the resistivity on cooling and heating near the step-like anomaly. The upper left inset presents the low-temperature heat capacity measured in zero magnetic field. The solid red line is a fit of the data (see the Experimental Section).

transition metal oxides.[48] Re_2Ga_9Ge exhibits metallic behavior, too. Furthermore, the low-temperature heat capacity data, which is shown in the inset of Figure 7, indicate the noticeable Sommerfeld coefficient of γ = 5.25(5) mJ mol^{-1} K^{-2} in agreement with the metallic nature of the compound. The experimental value of γ is larger than the value of γ_{bare} = 3.1 mJ mol^{-1} K^{-2} calculated for the ordered model, which may indicate electronic correlations in the system.

Figure 8 summarizes thermal transport properties of Re_2Ga_9Ge. The Seebeck coefficient is negative and decreases with increasing temperature. The room-temperature value of S = −3.5 μV/K is in good agreement with the observed metallic behavior. Notably, Re_2Ga_9Ge demonstrates low thermal conductivity: the measured values are below 2 W·m^{-1}·K^{-1} in the studied temperature range. Note that thermal conductivity of less than 2 W·m^{-1}·K^{-1} favors promising thermoelectric properties; thus, the value of thermal conductivity of typical metals usually reaches several tens of W·m^{-1}·K^{-1}, while the prospective thermoelectric materials have the κ of 0.5−3 W·m^{-1}·K^{-1}.[49] The electronic contribution to the total thermal conductivity can be calculated using the Wiedemann−Franz law, $\kappa_e = LT/\rho$, where L = 2.44 × 10^{-8} W·Ω·K^{-2} is the ideal Lorentz number, T is the absolute temperature, and ρ is the measured electrical resistivity. Clearly, the electronic and

https://doi.org/10.1021/acs.inorgchem.1c03240
Inorg. Chem. 2022, 61, 568−578

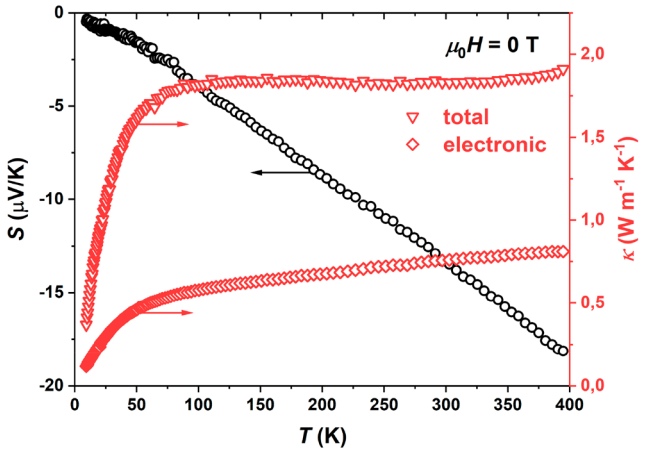

Figure 8. Seebeck coefficient (left axis) and thermal conductivity (right axis) of Re_2Ga_9Ge.

lattice contributions are comparable with each other and do not exceed 1 $W \cdot m^{-1} \cdot K^{-1}$ at T = 400 K, indicating interesting thermal transport properties of Re_2Ga_9Ge. In turn, low phonon thermal conductivity can be explained by the effective phonon scattering provided by heavy rhenium atoms, which are located in relatively large gallium polyhedra. However, because of a relatively low Seebeck coefficient typical for metals, the thermoelectric figure-of-merit does not exceed $ZT = 5 \times 10^{-3}$.

CONCLUSIONS

A new endohedral gallium cluster compound, Re_2Ga_9Ge, was discovered in the Re−Ga−Ge ternary system using the crystal growth joint flux technique by employing the excess of gallium and germanium. Crystals of the previously unknown phase were found in a mixture with the $ReGa_{5-y}Ge_y$ solid solution. Further synthesis of the Re_2Ga_9Ge polycrystalline sample confirmed the formation of the title compound. We note that the joint flux technique is a powerful tool for the exploratory synthesis and should be further employed for the search of new representatives of the endohedral gallium cluster compounds in related ternary systems.

Re_2Ga_9Ge crystallizes in an unknown structure type, in which rhenium-filled endohedral gallium clusters form a framework together with chains of tetrahedra composed purely of *p*-metal atoms. The chemical bonding pattern is based on two-center interactions between gallium and germanium and multicenter bonds involving *d*-orbitals of rhenium. The Fermi level is located in a pronounced pseudogap of the density of states, indicating that valence electron count is close to optimal. The compound exhibits metallic properties with an indication of electronic phase transition. This transition may be driven by the charge ordering, which once again underlines the peculiar chemical bonding in Re_2Ga_9Ge. Although no transition to the superconducting state was observed, the discovery of a new endohedral cluster compound and analysis of its crystal and electronic structure add to our knowledge of this type of intermetallic compounds and provide new pathways to the search for superconductors with unconventional properties.

ASSOCIATED CONTENT

Supporting Information

The Supporting Information is available free of charge at https://pubs.acs.org/doi/10.1021/acs.inorgchem.1c03240.

Crystallographic and refinement parameters for Re_2Ga_9Ge powder sample, PXRD patterns of crystals obtained from gallium flux, results of DSC, and comparison of calculated DOS without and taking into account spin−orbital coupling for Re_2Ga_9Ge (PDF)

Accession Codes

CCDC 2108772 and 2117048 contain the supplementary crystallographic data for this paper. These data can be obtained free of charge via www.ccdc.cam.ac.uk/data_request/cif, or by emailing data_request@ccdc.cam.ac.uk, or by contacting The Cambridge Crystallographic Data Centre, 12 Union Road, Cambridge CB2 1EZ, UK; fax: +44 1223 336033.

AUTHOR INFORMATION

Corresponding Author

Andrei V. Shevelkov − *Department of Chemistry, Lomonosov Moscow State University, 119991 Moscow, Russia;* orcid.org/0000-0002-8316-3280; Email: shev@inorg.chem.msu.ru

Authors

Maxim S. Likhanov − *Department of Chemistry, Lomonosov Moscow State University, 119991 Moscow, Russia;* orcid.org/0000-0002-4683-8197

Valeriy Yu. Verchenko − *Department of Chemistry, Lomonosov Moscow State University, 119991 Moscow, Russia; National Institute of Chemical Physics and Biophysics, 12618 Tallinn, Estonia;* orcid.org/0000-0002-8000-425X

Vladislav O. Zhupanov − *Department of Chemistry, Lomonosov Moscow State University, 119991 Moscow, Russia*

Zheng Wei − *Department of Chemistry, University at Albany, SUNY, Albany, New York 12222, United States*

Evgeny V. Dikarev − *Department of Chemistry, University at Albany, SUNY, Albany, New York 12222, United States;* orcid.org/0000-0001-8979-7914

Alexey N. Kuznetsov − *Department of Chemistry, Lomonosov Moscow State University, 119991 Moscow, Russia; N. S. Kurnakov Institute of General and Inorganic Chemistry RAS, 119991 Moscow, Russia;* orcid.org/0000-0002-3138-1569

Complete contact information is available at: https://pubs.acs.org/10.1021/acs.inorgchem.1c03240

Author Contributions

The manuscript was written through contributions of all authors.

Notes

The authors declare no competing financial interest.

ACKNOWLEDGMENTS

This work was supported by the Russia Science Foundation, grant # 17-13-01033. Electronic structure calculations were partially carried out using the equipment of the shared research facilities of the HPC computing resources at Lomonosov Moscow State University. The single-crystal study at UAlbany

has been funded by the National Science Foundation, grant no. CHE-1955585.

REFERENCES

(1) Verchenko, V. Yu; Shevelkov, A. V. Endohedral cluster intermetallic superconductors: at the frontier between chemistry and physics. *Dalton Trans.* **2021**, *50*, 5109−5114.

(2) Lobring, K. C.; Check, C. E.; Znang, J.; Li, S.; Zheng, C.; Rogacki, K. Single crystal growth, bonding analysis and superconductivity of V_2Ga_5. *J. Alloys Compd.* **2002**, *347*, 72−78.

(3) Xie, W.; Luo, H.; Phelan, B. F.; Klimczuk, T.; Cevallos, F. A.; Cava, R. J. Endohedral gallide cluster superconductors and superconductivity in $ReGa_5$. *Proc. Natl. Acad. Sci. U. S. A.* **2015**, *112*, E7048−E7054.

(4) Shibayama, T.; Nohara, M.; Katori, H. A.; Okamoto, Y.; Hiroi, Z.; Takagi, H. Superconductivity in Rh_2Ga_9 and Ir_2Ga_9 without Inversion Symmetry. *J. Phys. Soc. Jpn.* **2007**, *76*, 073708.

(5) Verchenko, V. Yu; Tsirlin, A. A.; Zubtsovskiy, A. O.; Shevelkov, A. V. Strong electron-phonon coupling in the intermetallic superconductor Mo_8Ga_{41}. *Phys. Rev. B: Condens. Matter Mater. Phys.* **2016**, *93*, 064501.

(6) Verchenko, V. Yu; Tsirlin, A. A.; Shevelkov, A. V. Semiconducting and superconducting Mo−Ga frameworks: total energy and chemical bonding. *Inorg. Chem. Front.* **2021**, *8*, 1702−1709.

(7) Häussermann, U.; Boström, M.; Viklund, P.; Rapp, Ö.; Björnängen, T. $FeGa_3$ and $RuGa_3$: Semiconducting Intermetallic Compounds. *J. Solid State Chem.* **2002**, *165*, 94−99.

(8) Likhanov, M. S.; Shevelkov, A. V. Intermetallic compounds with non-metallic properties. *Russ. Chem. Bull.* **2020**, *69*, 2231−2250.

(9) Ryżyńska, Z.; Wiśniewski, P.; Kaczorowski, D.; Xia, W.; Cava, R. J.; Klimczuk, T.; Winiarski, M. Superconductivity in the Endohedral Ga Cluster Compound $PdGa_5$. *J. Phys. Chem. C* **2021**, *125*, 11294−11299.

(10) Bezinge, A.; Yvon, K.; Decroux, M.; Muller, J. On the existence of binary Mo_8Ga_{41} and its properties. *J. Less-Common Met.* **1984**, *99*, L27−L31.

(11) Wollmann, L.; Nayak, A. K.; Parkin, S. S. P.; Felser, C. Heusler 4.0: Tunable Materials. *Annu. Rev. Mater. Res.* **2017**, *47*, 247−270.

(12) Yannello, V. J.; Fredrickson, D. C. Orbital Origins of Helices and Magic Electron Counts in the Nowotny Chimney Ladders: the 18 − n Rule and a Path to Incommensurability. *Inorg. Chem.* **2014**, *53*, 10627−10631.

(13) Yannello, V. J.; Fredrickson, D. C. Generality of the 18-n Rule: Intermetallic Structural Chemistry Explained through Isolobal Analogies to Transition Metal Complexes. *Inorg. Chem.* **2015**, *54*, 11385−11398.

(14) Fredrickson, D. C. Parallels in Structural Chemistry between the Molecular and Metallic Realms Revealed by Complex Intermetallic Phases. *Acc. Chem. Res.* **2018**, *51*, 248−257.

(15) Verchenko, V. Yu; Khasanov, R.; Guguchia, Z.; Tsirlin, A. A.; Shevelkov, A. V. Two-gap superconductivity in Mo_8Ga_{41} and its evolution upon vanadium substitution. *Phys. Rev. B: Condens. Matter Mater. Phys.* **2017**, *96*, 134504.

(16) Verchenko, V. Yu; Zubtsovskii, A. O.; Tsirlin, A. A.; Wei, Zh.; Roslova, M.; Dikarev, E. V.; Shevelkov, A. V. Mo_6Ga_{31} endohedral cluster superconductor. *J. Alloys Compd.* **2020**, *848*, 156400.

(17) Verchenko, V. Yu; Zubtsovskii, A. O.; Wei, Zh.; Tsirlin, A. A.; Dikarev, E. V.; Shevelkov, A. V. From endohedral cluster superconductors to approximant phases: synthesis, crystal and electronic structure, and physical properties of $Mo_8Ga_{41-x}Zn_x$ and $Mo_7Ga_{52-x}Zn_x$. *Dalton Trans.* **2019**, *48*, 7853−7861.

(18) Verchenko, V. Yu; Zubtsovskii, A. O.; Wei, Zh.; Tsirlin, A. A.; Marcin, M.; Sobolev, A. V.; Presniakov, I. A.; Dikarev, E. V.; Shevelkov, A. V. Endohedral Cluster Superconductors in the Mo−Ga−Sn System Explored by the Joint Flux Technique. *Inorg. Chem.* **2019**, *58*, 15552−15561.

(19) Verchenko, V. Yu; Zubtsovskii, A. O.; Plenkin, D. S.; Bogach, A. V.; Wei, Zh.; Tsirlin, A. A.; Dikarev, E. V.; Shevelkov, A. V. Family of Mo_4Ga_{21}-Based Superconductors. *Chem. Mater.* **2020**, *32*, 6730−6735.

(20) Verchenko, V. Yu; Mironov, A. V.; Wei, Zh.; Tsirlin, A. A.; Dikarev, E. V.; Shevelkov, A. V. Crystal Growth of Intermetallics from the Joint Flux: Exploratory Synthesis through the Control of Valence Electron Count. *Inorg. Chem.* **2019**, *58*, 1561−1570.

(21) Marshall, M.; Górnicka, K.; Dissanayaka Mudiyanselage, R. S.; Klimczuk, T.; Xie, W. New Tetragonal $ReGa_5(M)$ (M = Sn, Pb, Bi) Single Crystals Grown from Delicate Electrons Changing. *Crystals* **2019**, *9*, 527.

(22) Likhanov, M. S.; Verchenko, V. Yu; Gippius, A. A.; Zhurenko, S. V.; Tkachev, A. V.; Wei, Z.; Dikarev, E. V.; Kuznetsov, A. N.; Shevelkov, A. V. Electron-Precise Semiconducting $ReGa_2Ge$: Extending the $IrIn_3$ Structure Type to Group 7 of the Periodic Table. *Inorg. Chem.* **2020**, *59*, 12748−12757.

(23) Likhanov, M. S.; Khalaniya, R. A.; Verchenko, V. Yu.; Gippius, A. A.; Zhurenko, S. V.; Tkachev, A. V.; Fazlizhanova, D. I.; Kuznetsov, A. N.; Shevelkov, A. V. $ReGaGe_2$: an intermetallic compound with semiconducting properties and localized bonding. *Chem. Commun.* **2019**, *55*, 5821−5824.

(24) Xie, W.; Gustin, L.; Bian, G. 111-Type Semiconductor ReGaSi Follows $14e^-$ Rules. *Inorg. Chem.* **2017**, *56*, 5165−5172.

(25) Decocq, V.; Gui, X.; Neeson, A.; Xie, W.; Heitmann, T.; Wang, F. Crystal Structures, Superconducting Properties, and the Coloring Problem in ReAlSi and ReGaSi. *Inorg. Chem.* **2020**, *59*, 17310−17319.

(26) *SAINT*, Version 8.38A; Bruker AXS, Inc.: Madison, Wisconsin, USA, 2018.

(27) *SADABS*, v. 2016/2; Bruker AXS, Inc.: Madison, WI, 2016.

(28) Krause, L.; Herbst-Irmer, R.; Sheldrick, C. M.; Stalke, D. Comparison of silver and molybdenum microfocus X-ray sources for single-crystal structure determination. *J. Appl. Crystallogr.* **2015**, *48*, 3−10.

(29) Palatinus, L.; Chapuis, G. SUPERFLIP - a computer program for the solution of crystal structures by charge flipping in arbitrary dimensions. *J. Appl. Crystallogr.* **2007**, *40*, 786−790.

(30) Sheldrick, G. M. Crystal structure refinement with SHELXL. *Acta Crystallogr., Sect. C: Struct. Chem.* **2015**, *C71*, 3−8.

(31) Momma, K.; Izumi, F. VESTA 3 for three-dimensional visualization of crystal, volumetric and morphology data. *J. Appl. Crystallogr.* **2011**, *44*, 1272−1276.

(32) Petříček, V.; Dušek, M.; Palatinus, L. Crystallographic Computing System JANA2006: General features. *Z. Kristallogr. - Cryst. Mater.* **2014**, *229*, 345−352.

(33) ELK, an all-electron full-potential linearised augmented-plane wave (FP-LAPW) code. http://elk.sourceforge.net (accessed 2021-12-19).

(34) Perdew, J. P.; Ruzsinszky, A.; Csonka, G. I.; Vydrov, O. A.; Scuseria, G. E.; Constantin, L. A.; Zhou, X.; Burke, K. Restoring the Density-Gradient Expansion for Exchange in Solids and Surfaces. *Phys. Rev. Lett.* **2008**, *100*, 136406.

(35) Bader, R. F. W. *Atoms in Molecules: A Quantum Theory*; Oxford University Press: Oxford, U.K., 1990.

(36) Kohout, M. A measure of electron localizability. *Int. J. Quantum Chem.* **2004**, *97*, 651−658.

(37) Kohout, M. Bonding indicators from electron pair density functionals. *Faraday Discuss.* **2007**, *135*, 43−54.

(38) Kohout, M.; Pernal, K.; Wagner, F. R.; Grin, Yu. Electron localizability indicator for correlated wavefunctions. I. Parallel-spin pairs. *Theor. Chem. Acc.* **2004**, *112*, 453−459.

(39) Kohout, M. *DGrid*, ver. 4.6; Radebeul, 2011.

(40) Scheie, A. LongHCPulse: Long-Pulse Heat Capacity on a Quantum Design PPMS. *J. Low Temp. Phys.* **2018**, *193*, 60−73.

(41) Likhanov, M. S.; Verchenko, V. Yu; Kuznetsov, A. N.; Shevelkov, A. V. $ReGa_{0.4}Ge_{0.6}$: Intermetallic Compound with Pronounced Covalency in the Bonding Pattern. *Inorg. Chem.* **2019**, *58*, 2822−2832.

(42) Bockelmann, W.; Schuster, H.-U. Ternäre Phasen im Dreistoffsystem Lithium-Gallium-Germanium. *Z. Anorg. Allg. Chem.* **1974**, *410*, 233−240.

https://doi.org/10.1021/acs.inorgchem.1c03240
Inorg. Chem. 2022, 61, 568−578

(43) Panday, P. K.; Schubert, K. Strukturuntersuchungen in einigen Mischungen T-B^3-B^4 (T = Mn, Fe, Co, Ir, Ni, Pd; B^3 = Al, Ga, Tl; B^4 = Si, Ge). *J. Less-Common Met.* **1969**, *18*, 175−202.
(44) Sharma, B. D.; Donohue, J. A. A refinement of the crystal structure of gallium. *Z. Kristallogr.* **1962**, *117*, 293−300.
(45) Evers, J.; Mayer, P.; Möckl, L.; Oehlinger, G.; Köppe, R.; Schnöckel, H. Two High-Pressure Phases of SiS_2 as Missing Links between the Extremes of Only Edge-Sharing and Only Corner-Sharing Tetrahedra. *Inorg. Chem.* **2015**, *54*, 1240−1253.
(46) Antonyshyn, I.; Prots, Yu.; Margiolaki, I.; Schmidt, M. P.; Zhak, O.; Oryshchyn, S.; Grin, Yu. Tetragonal-antiprismatic coordination of transition metals in intermetallic compounds: ω_1-Mn_6Ga_{29} and its structuralrelationships. *J. Solid State Chem.* **2013**, *199*, 141−148.
(47) Bain, G. A.; Berry, J. F. Diamagnetic Corrections and Pascal's Constants. *J. Chem. Educ.* **2008**, *85*, 532.
(48) Coey, M. Charge-ordering in oxides. *Nature* **2004**, *430*, 155−157.
(49) Shi, X.-L.; Chen, Zh.-G. Advanced Thermoelectric Design: From Materials and Structures to Devices. *Chem. Rev.* **2020**, *120*, 7399−7515.

https://doi.org/10.1021/acs.inorgchem.1c03240
Inorg. Chem. 2022, 61, 568−578